Dynamic tensile properties of reduced-activation ferritic steel F82H

AUTHOR(S):

Kasada, Ryuta; Ishii, Daiki; Ando, Masami; Tanigawa, Hiroyasu; Ohata, Mitsuru; Konishi, Satoshi

CITATION:

Kasada, Ryuta ...[et al]. Dynamic tensile properties of reduced-activation ferritic steel F82H. Fusion Engineering and Design 2015, 100: 146-151

ISSUE DATE:

2015-11

URL:

http://hdl.handle.net/2433/202564

Dynamic tensile properties of reduced-activation ferritic steel F82H

Ryuta KASADA[1*], Daiki ISHII[1], Masami ANDO[2], Hiroyasu TANIGAWA[2], Mitsuru OHATA[3], Satoshi KONISHI[1]

[1]*Institute of Advanced Energy, Kyoto University, Uji, Kyoto 611-0011, Japan*
[2]*Japan Atomic Energy Agency, Rokkasho, Aomori 039-3212, Japan*
[3]*Graduate School of Engineering, Osaka University, Suita, Osaka 565-0871, Japan*

*Corresponding Author:	Ryuta Kasada
Affiliation:	Institute of Advanced Energy, Kyoto University
Complete Mail Address:	Gokasho, Uji, Kyoto 611-0011, Japan
Email:	r-kasada@iae.kyoto-u.ac.jp
Telephone Number:	+81-774-38-3431
Fax Number:	+81-774-38-3439

Keyword: dynamic tensile properties, high-speed tensile test, reduced-activation ferritic steel, deformation

Abstract

The dynamic tensile properties of reduced-activation ferritic steel F82H was characterized by high-speed tensile tests over a strain-rate range of 0.01 to 1400 s^{-1} at temperatures of 296 and 423 K. As a result, the tensile strength of the F82H steel appears to be sensitive to strain-rate. This is explained by the activation volume of gliding dislocation. The uniform elongation is also sensitive to strain-rate but true fracture strain is considered to be less sensitive. Zerilli–Armstrong bcc model is found adequate to describe the dependence of yield stress of F82H on temperature and strain-rate tested in the present study.

1. Introduction

Plasma disruption events will give large and transient electromagnetic forces on the structural materials of tokamak machines including ITER [1]. It is obvious that strain-rate in the structural materials during plasma disruption events is a design-dependent and operation-dependent parameter. Assuming that plasma current of 16.7 MA linearly decreases in 30 ms, for example, Tanigawa et al. calculated the Eddy current distribution and subsequent electromagnetic forces in the DEMO blanket [2]. If the blanket structure has a few millimeter thickness, estimated strain-rate during current plasma disruption event is ~0.1 s^{-1}. While available information of the structural design is limited, a possible

strain-rate window of structural materials in fusion reactor is suggested in Fig. 1 which is based on the Lindholm diagram [3]. Divertor components in magnetic fusion machines may receive high strain-rates due to short pulse thermal loading from edge localized mode (ELM) [4]. Solid wall of laser inertial fusion reactor may suffer from much higher strain-rates due to the pulse loading [5]. These facts motivate high strain-rate testing to investigate the dynamic mechanical properties of fusion reactor materials.

Dynamic mechanical properties under high strain-rates are very important for the structural integrity of nuclear power plants. Reference fracture toughness procedures applied to pressure vessel steels of fission nuclear reactors considers dynamic fracture toughness [6,7]. Therefore safety management of DEMO and commercial fusion reactor in future will demand evaluation and prediction of dynamic deformation and fracture properties of fusion reactor materials. European group has reported the first results on the dynamic fracture toughness of a reduced-activation ferritic (RAF) steel EUROFER before and after neutron irradiation using master curve method [8]. The results showed that reference temperature of dynamic condition is higher of approximately 70 K than that of static condition. It was also notable that the shift of reference temperature of dynamic condition is similar with that of static condition. These results strongly offer to investigate the fundamental process of deformation and fracture of RAF steels under dynamic condition.

Generally, the tensile strength and toughness of bcc alloys have significant temperature dependence [9]. Considering the thermal activation process of gliding dislocation responsible to the deformation, high strain-rate may have an impact on the mechanical properties of RAF steels. In fact, EUROFER showed a significant strain-rate dependence of tensile properties at the ambient temperature [10]. However there is no sufficient data of dynamic tensile properties and dynamic fracture toughness of F82H. The present study shows first results of the dynamic tensile deformation behavior of RAF steel F82H.

2. Experimental procedure

The material used in this study is F82H BA-07 heat [11]. As shown in Fig. 2, Small round bar specimens, the gauge of which is 10 mm in length and 2 mm in diameter, were fabricated for high-speed tensile tests using Hydroshot HITS-T10, SHIMADZU Corporation [12]. The Hydroshot machine uses a servo-hydraulic system to achieve a maximum actuator speed of 20 m/s. Testing temperatures were 296 K and 423 K. The displacement among the chucks was precisely acquired by an Eddy current extensometer which is a noncontact device capable of the position measurement. Experiments at a room temperature of 296 K were carried out at strain-rates of 0.01, 1, 10, 100, and 1400 s^{-1}. Experiments at a room temperature of 423 K were carried out at strain-rates of 0.01, 100, and 1400 s^{-1}.

Fracture surface was observed by scanning electron microscopy (SEM) using JEOL JSM-5600LV.

Deformation microstructure was observed by transmission electron microscopy (TEM) JEOL JEM-2100F. Focused ion beam (FIB) device HITACH FB-2100 was used for making samples from the deformed area as shown in Fig. 3.

3. Results and discussion

Nominal stress-strain curves of F82H steel obtained by the high-speed tensile tests were shown in Fig. 4 (a) at 296 K and (b) at 423 K. The highest strain-rate tests of 1400 s^{-1} show oscillation of load signal due to ringing of the loading system but the reproducibility is good. The results clearly show strain-rate sensitivity in the both of strength and elongation at 296 and 423K. Notably, both of the nominal tensile strength and nominal fracture strain increased with strain-rate.

Fig. 5 shows 0.2% off-set yield stress and ultimate tensile strength (UTS) against strain-rate in log scale. From a dislocation mechanics viewpoint [13], activation volume V of gliding dislocation can be deduced from the gradient of strain-rate dependence of the yield stress conventionally as following equation,

$$V = MkT \frac{d \ln \dot{\varepsilon}}{d\sigma_y} \quad (1),$$

where k is Boltzmann's constant, T is a testing temperature, $\dot{\varepsilon}$ is a strain-rate, σ_y is a 0.2% off-set yield stress and M is Tailor's factor (M=3.06). Table 1 shows the calculated activation volumes described by a scale of Burger's vector (b=0.286 nm). At the higher strain-rate region over 10 s^{-1}, the small activation volume can be responsible for the kink-pair formation probability [14]. At the lower strain-rate region, the higher activation volume is possibly due to the interaction between gliding dislocation and dislocation forest. These results indicate that the high strain-rate changed the deformation mode of F82H steel even at room temperature.

Table 1 Activation volume of gliding dislocation at 296 and 423 K.

Testing temperature (K)	Lower strain-rate(s^{-1})	Higher strain-rate (s^{-1})	Activation volume (m^3)
296	0.01	1	$75b^3$
	1	10	$56b^3$
	10	100	$19b^3$
	100	1400	$17b^3$
423	0.01	100	$98b^3$
	100	1400	$26b^3$

Full set of true stress-strain curves of F82H IEA-heat at normal strain-rate conditions were precisely obtained by Shiba and Hirose [15]. Here true stress-strain curves and strain hardening

exponent *n* of F82H BA07-heat up to an occurrence of necking at UTS were conventionally calculated from the nominal stress-strain curves and were plotted in Fig. 6. In general, reduction in strain hardening induces necking earlier and can decrease uniform strain (e.g. [16]). However F82H steel showed that true strain at stating of necking, i.e. uniform strain, at 296 K decreased with increasing strain rates from 0.01 to 0.1 s^{-1}, and then increased with strain-rate above 1 s^{-1}. Strain hardening exponents at 296 K increased with increasing strain-rate from 0.01 to 10 s^{-1}, and then decreased with strain-rate above 10 s^{-1}. While it is difficult to find a similar strain-rate effect on uniform strain of other ferritic steels, some papers have indicated that increasing of strain-rate increases fracture strain of TRIP (transformation induced plasticity)-type steels (e.g. [16]). Fig. 7 shows fracture surface of high-speed tensile test specimens at (a) 296 K and (b) 423 K , and (c) plots of reduction of area calculated from the fracture surface. No significant difference of reduction of area was observed in the fracture surfaces among the different strain-rate conditions. Therefore the higher nominal fracture strain of F82H steel under higher strain-rate tensile tests is attributed to the increment of uniform strain. This means that true fracture strain of F82H steel was not affected by the nominal strain-rate. Fig. 8 shows deformation microstructure near the fracture surface observed by TEM of normal (0.01 s^{-1}) and high (1400 s^{-1}) strain-rate conditions, indicating no clear difference between them. Nanostructured fcc metals and alloys has shown this kind of “positive” effect of strain-rate on ductility. Wang and Ma suggested that ductility of these materials was improved due to multi-modal grain size distribution, a uniform and efficient storage of dislocations under cryo-rolling, and elevated strain-rate sensitivity [17]. Althouh no clear microstructural evidence was obtained, the activation volume analysis shown in Table 1 suggests that uniform and efficient storage of plastic-deformation source such as kink-pair formation as well as high strain-rate sensitivity may be responsible for the positive effect of strain-rate on uniform strain of of F82H steel.

Constitutive equation including the high strain-rate regime should be established for engineering design of blanket structure. Liang and Khan reviewed four kinds of constitutive models and pointed out that these models are inadequate to describe the decreasing of strain hardening rate with increasing strain-rate as seen in the present F82H [18]. Therefore these models can be used to predict not UTS but the yield stress. Here the Zerilli–Armstrong bcc model is examined to predict yield stress as a following equation:

$$\sigma_y = \sigma_0 + \sigma_1 \exp\left[-\left(\alpha - \beta \ln \dot{\varepsilon}\right)T\right] \quad (3),$$

where σ_0 is the athermal stress component and σ_1 is the pre-exponetial coefficient of thermal stress, α is the thermal softening coefficient, and β is the coefficient of the temperature and strain-rate coupling term. Fig. 9 shows 0.2%-offset yield stress σ_y against T and log $\dot{\varepsilon}$ with a surface fitting result based on the Zerilli–Armstrong bcc model (σ_0 = 535 MPa, σ_1 = 3536 MPa, α = 1.38 × 10^{-2} K^{-1}, β =6.30 × 10^{-4} K^{-1}). In addition to the present high-speed tensile test results,

the surface fitting used a set of experimental data at low temperatures below 200 K with a strain rate of 8.0×10^{-4} s^{-1} as plotted in the figure [19]. Correlation with the experimental data is good for the wide range of strain-rate tested in the present study.

The results obtained here will be used to investigate dynamic fracture toughness of F82H. Further study on the strain-rate effect on neutron-irradiated materials is also needed. In addition, the high strain-rate test results give a valuable implication to understand irradiation-induced ductility-loss followed by irradiation hardening. Irradiation hardening induces non-uniform deformation through the dislocation channeling and decrease of strain hardening [20,21]. In this case, plastic deformation concentrates into small area which leads to higher true strain-rate in the deformed area. Such effect will be investigated in future study.

4. Conclusion

We found strain-rate dependence of tensile properties of F82H BA07-heat by high-speed tensile testing at 296 K and 423 K. Test results are summarized as bellows:

(1) The result clearly shows higher strength for higher strain-rate condition. The activation volume analysis suggests a change of deformation mechanism at around 10-100 s^{-1}.

(2) Higher strain-rate condition testing resulted in the higher uniform strain. In contrast, reduction of area indicates similar true fracture strain among the present strain-rate conditions.

(3) Zerilli–Armstrong bcc model can predict dependence of yiled stress of F82H steel on temperature and strain-rate tested in the present study.

Acknowledgements

The authors would like to thank Mr. Daigen, Shimadzu Co., for his kind support on the high-speed tensile tests.

References

[1] J.D. Kotulski, R.S. Coats, M.F. Pasik, Fusion Eng. Design 83 (2008) 1068–1071.

[2] Hiroyasu Tanigawa, Hisashi Tanigawa, M. Ando, S. Nogami, T. Hirose, D. Hamaguchi, T. Nakata, H. Sakasegawa, M. Enoeda, Y. Someya, H. Utoh, K. Tobita, K. Ochiai, C. Konno, R. Kasada, A.Möslang, E. Diegele, M.A. Sokolov, L.L. Snead, Y. Katoh, R.E. Stoller, S.J. Zinkle, “Research and Development Status of Reduced Activation Ferritic/Martensitic Steels Corresponding to DEMO Design Requirement”, FTP/P7-17, Proceedings of the 24th IAEA Fusion Energy Conference San Diego, USA 8-13 October 2012.

[3] U.S. Lindholm, “High strain rate test”, Measurement of mechanical properties, Vol. 5, Techniques of Metals Research, Wiley Interscience (1971)

[4] I. Uytdenhouwen1, R. Chaouadi, J. Linke, V. Massaut and G. Van Oost, Advanced Materials

Research 59 (2009) 319–325.
[5] T. Goto, Y. Someya, Y. Ogawa, R. Hiwatari, Y. Asaoka, K Okano, A. Sunahara and T. Johzaki, Nucl. Fusion 49 (2009) 075006.
[6] American Society of Mechanical Engineers, Section III, “Rules for construction of nuclear facility components”, ASME’s Boiler and Pressure Vessel Code (2010).
[7] Japan Electric Association's standard JEAC 4206 (2007).
[8] M. Kytka, M. Brumovsky, M. Falcnik, J. Nucl. Mater. 409 (2011) 147–152.
[9] R. Liang, A.S. Khan, International Journal of Plasticity 15 (1999) 963–980.
[10] E. Cadoni, M. Dotta, D. Forni, P. Spatig, J. Nucl. Mater. 414 (2011) 360-366.
[11] H. Tanigawa, K. Shiba, H. Sakasegawa, T. Hirose, S. Jitsukawa, Fusion Engineering and Design 86 (2011) 2549–2552.
[12] T. Takii, Kensa-Gijutsu, 8 (2003) 51–56.
[13] P. Spätig, G.R. Odette, G.E. Lucas, Journal of Nuclear Materials 275 (1999) 324–331.
[14] D. Caillard, Acta Materialia 58 (2010) 3493–3503.
[15] K. Shiba, T. Hirose, Fusion Engineering and Design 81 (2006) 1051–1055.
[16] Y. Gao, J. Ahlström, B. Karlsson, Journal of Engineering Materials and Technology 133 (2011) 021019-1.
[17] Y.M. Wang, E. Ma, Acta Materialia 52 (2004) 1699–1709.
[18] R. Liang, A.S. Khan, International Journal of Plasticity 15 (1999) 963-980.
[19] Y. Ueda, Evaluation of fracture toughness using small specimens, Unpublished master's thesis, Osaka University, Japan (in Japanese), 2014.
[20] N. Hashimoto, S.J. Zinkle, R.L. Klueh, A.R. Rowcliffe, K. Shiba, Mat. Res. Soc. Symp. Proc., 650 (2001), p. R1.10.1.
[21] T.S. Byun, K. Farrell, Acta Materialia 52 (2004) 1597–1608.

Figure captions

Fig. 1 Dynamic aspects of mechanical testing and related phenomenon in general and in fusion reactor.
Fig.2 Clamping fixtures of the high-speed tensile test specimen.
Fig. 3 A FIBed specimen for TEM lifted out from deformaed tensile specimen.
Fig. 4 Engineering stess-strain curves obtained from tensile tests at different strain-rates at temperatures of (a) 296 K and (b) at 423 K.
Fig. 5 0.2% off-set yield stress and UTS against strain-rate in log scale in order to calculate the activation volumes at lower and higher strain-rates.
Fig. 6 True stress-strain curves and work-hardening coefficients calculated from Fig. 3.
Fig. 7 SEM fractography of fracture surfaces on (a) 296 K and (b) 423K, and (c) reduction of area

measured from (a) and (b).

Fig. 8 TEM micrographs of deformed area after tensile tests at 296 K for strain-rates of (a) 0.01 s^{-1} and (b) 1400 s^{-1}.

Fig. 9 Surface fitting result as shown meshed surface using the Zerilli–Armstrong bcc model to the experimental data of 0.2% off-set yield stress of F82H at differeint temperatures and different strain rates.

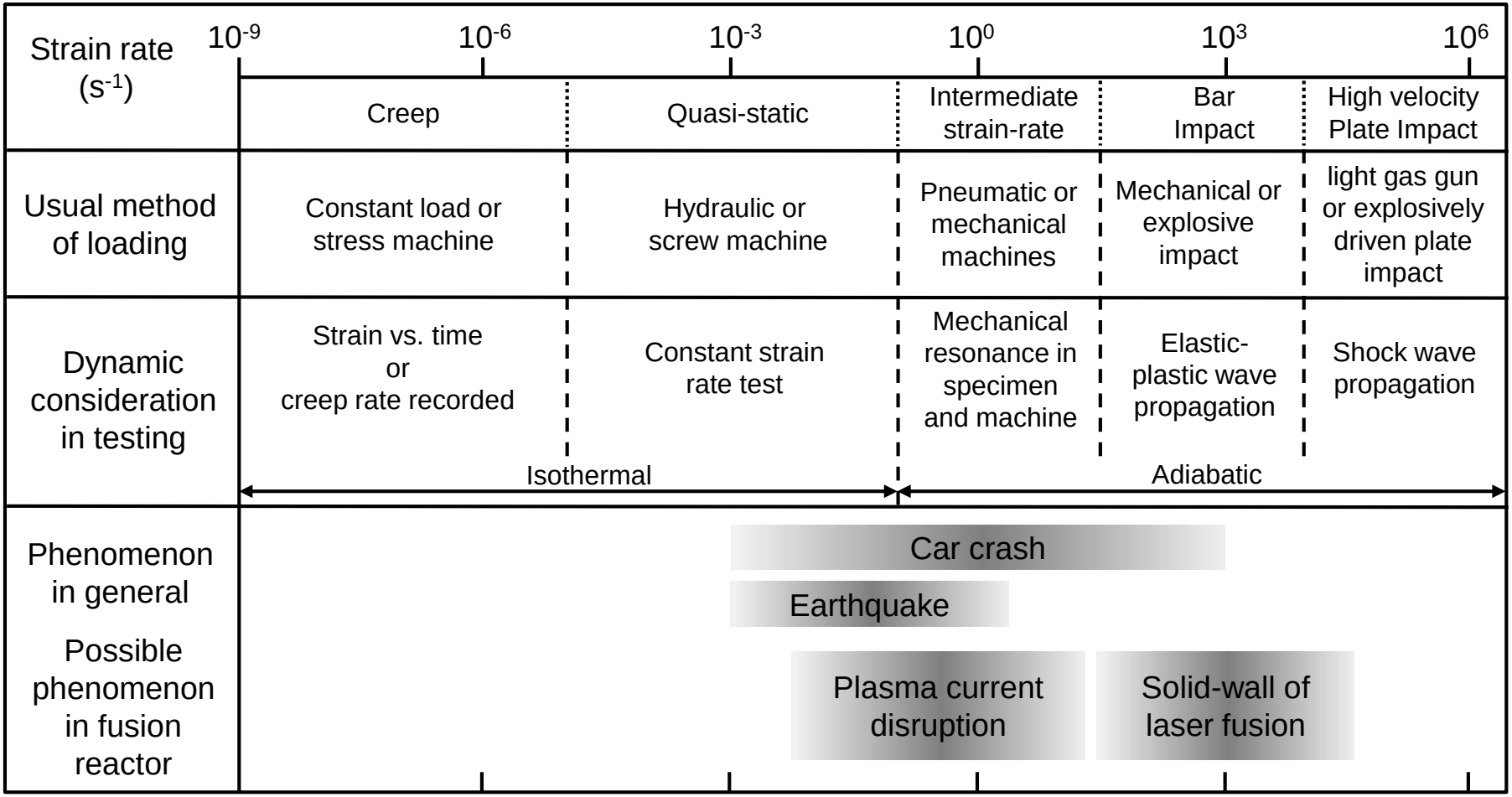

Based on U.S. Lindholm, “High strain rate test”, Measurement of mechanical properties, Vol. 5, Techniques of Metals Research, Wiley Interscience (1971)

Fig. 1

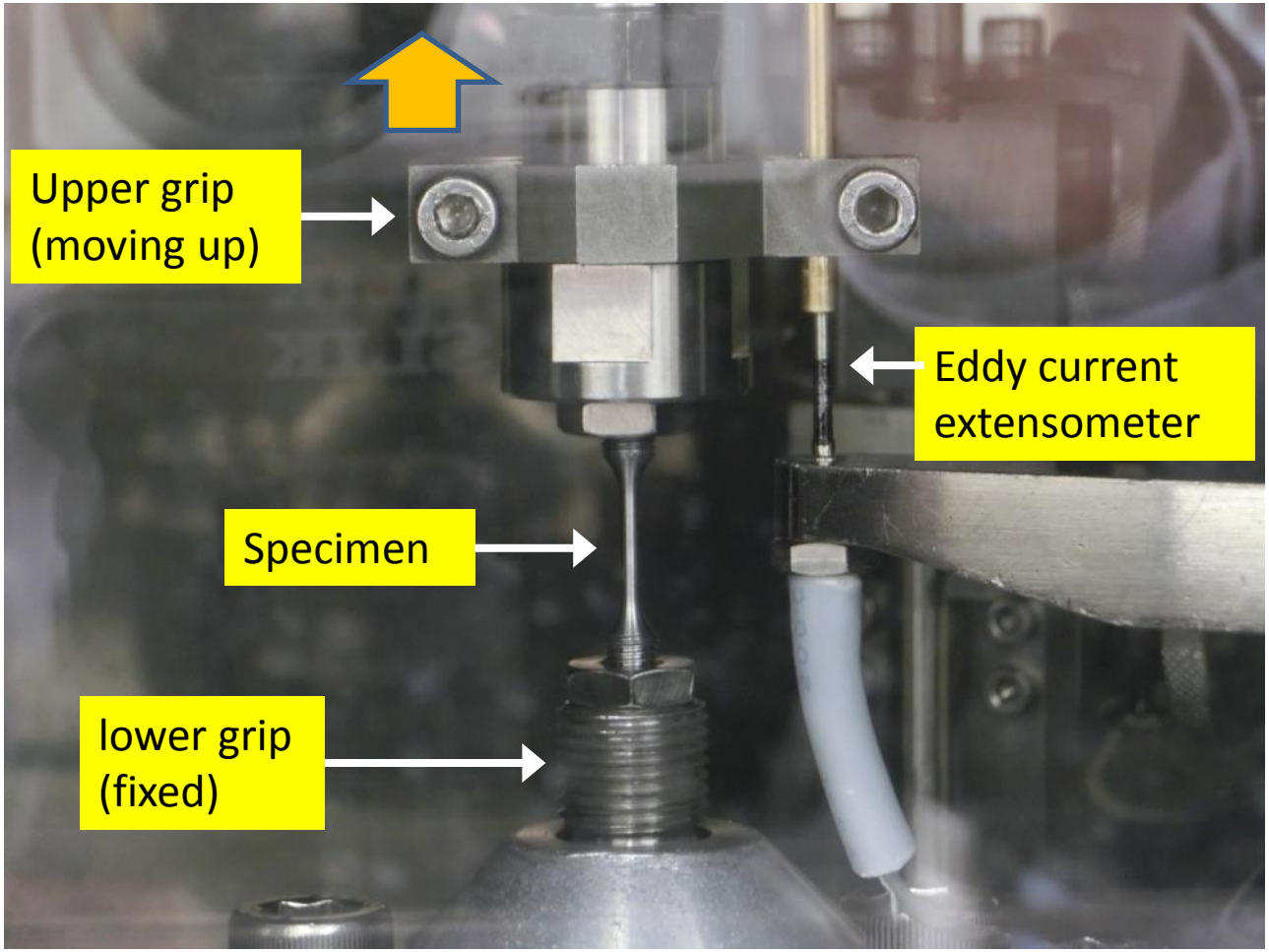

Fig. 2

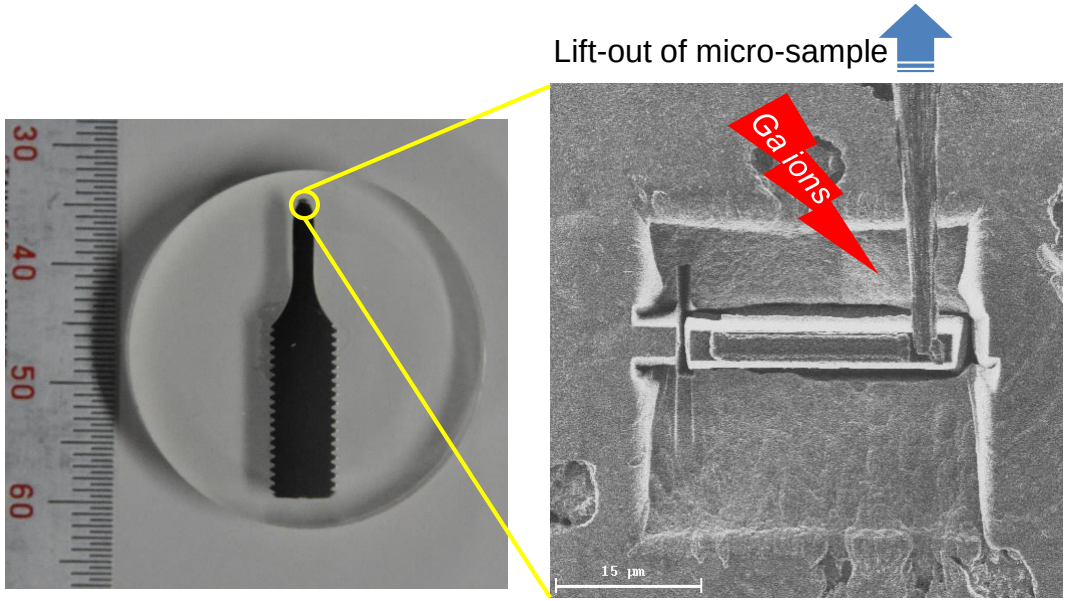

Mechanically-polished cross-sectional specimen

FIBed specimen for TEM

Fig. 3

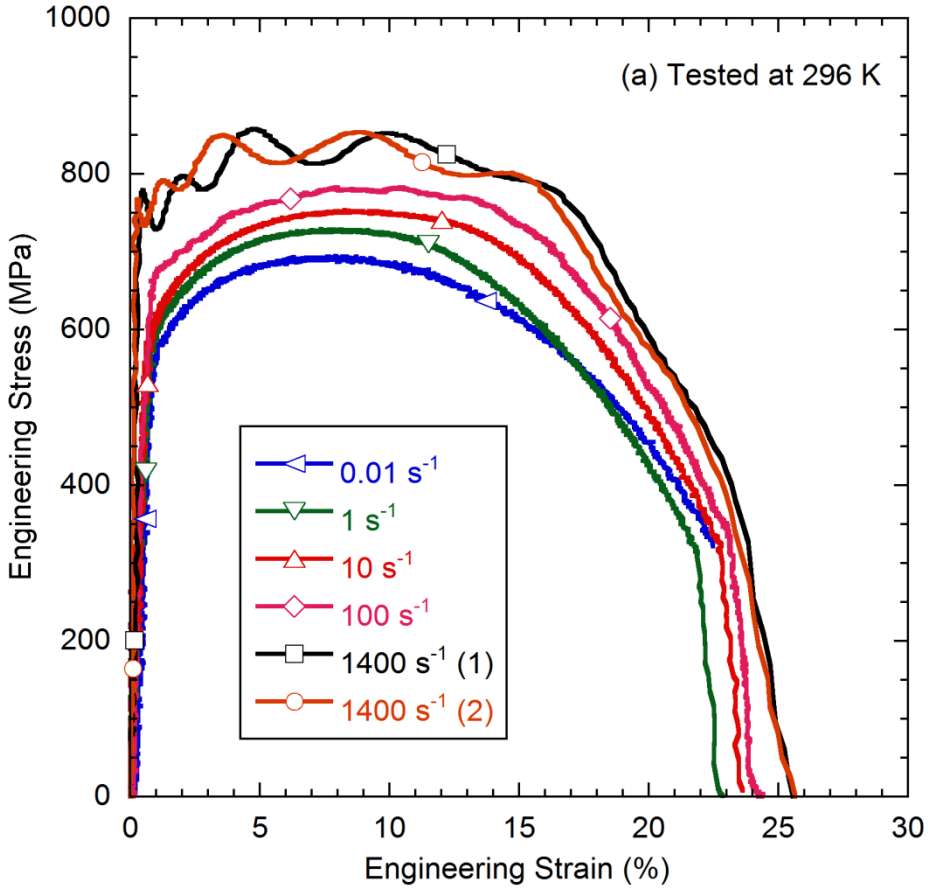

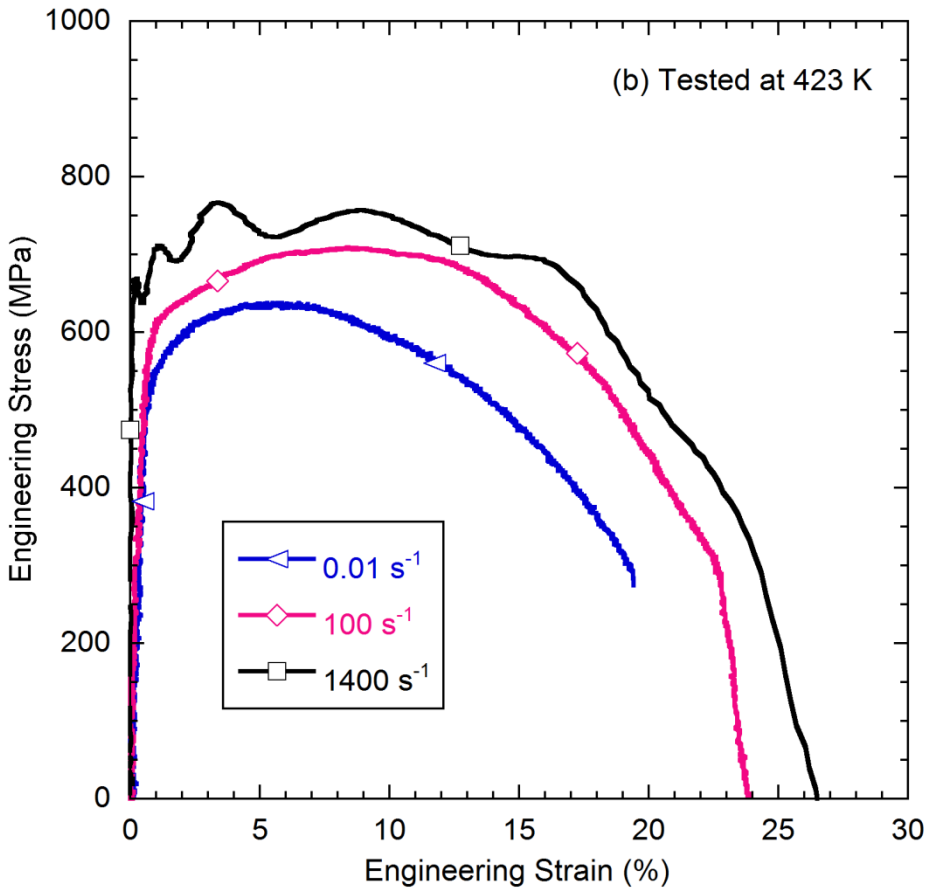

Fig. 4

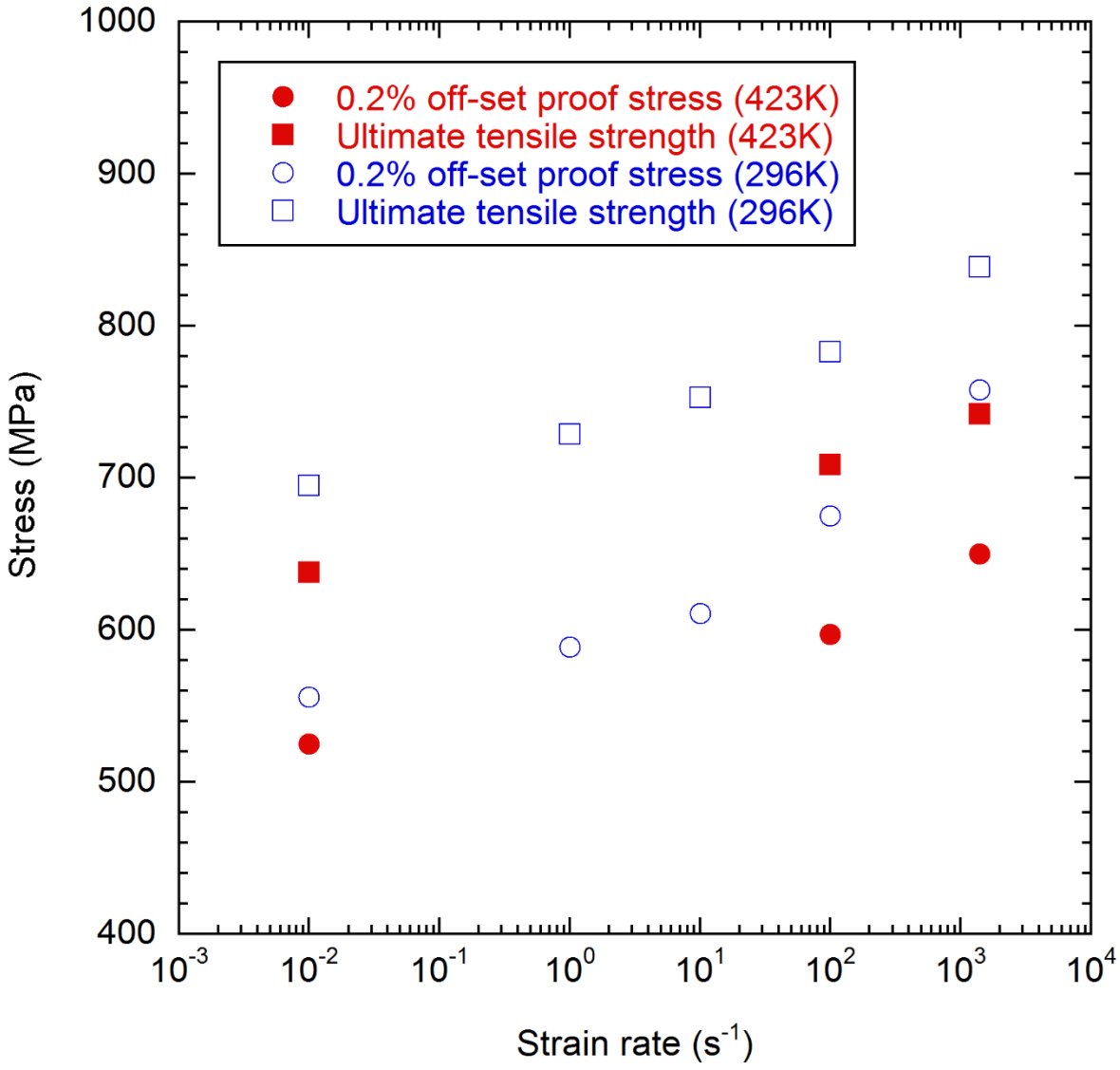

Fig. 5

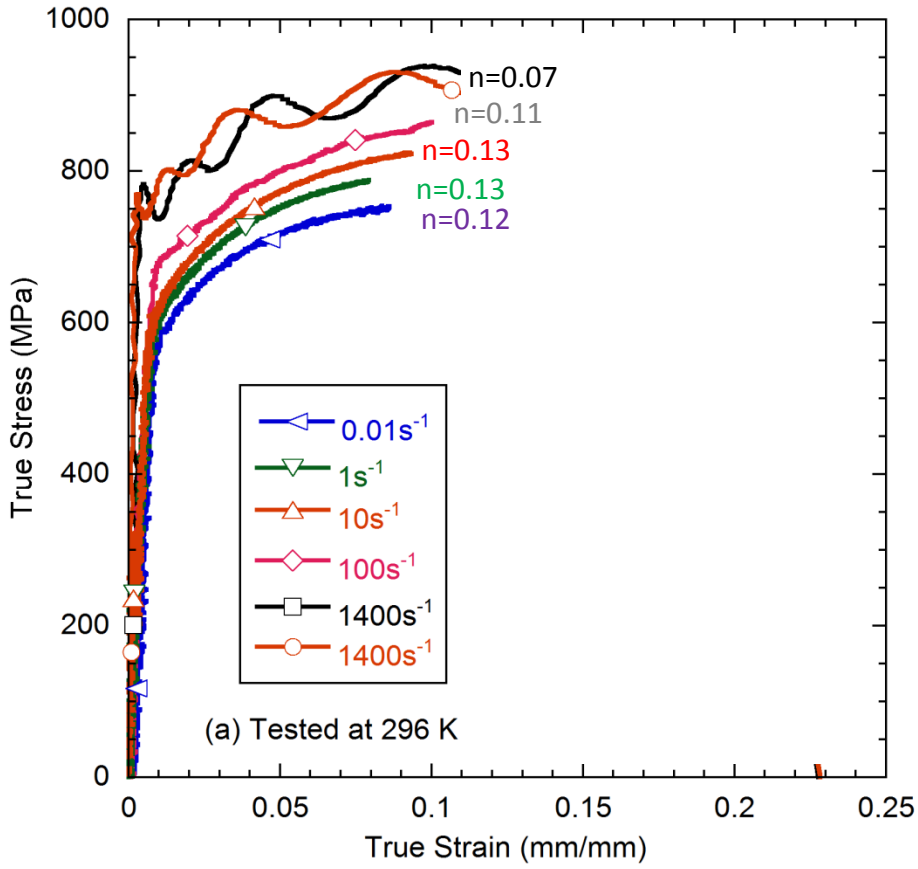

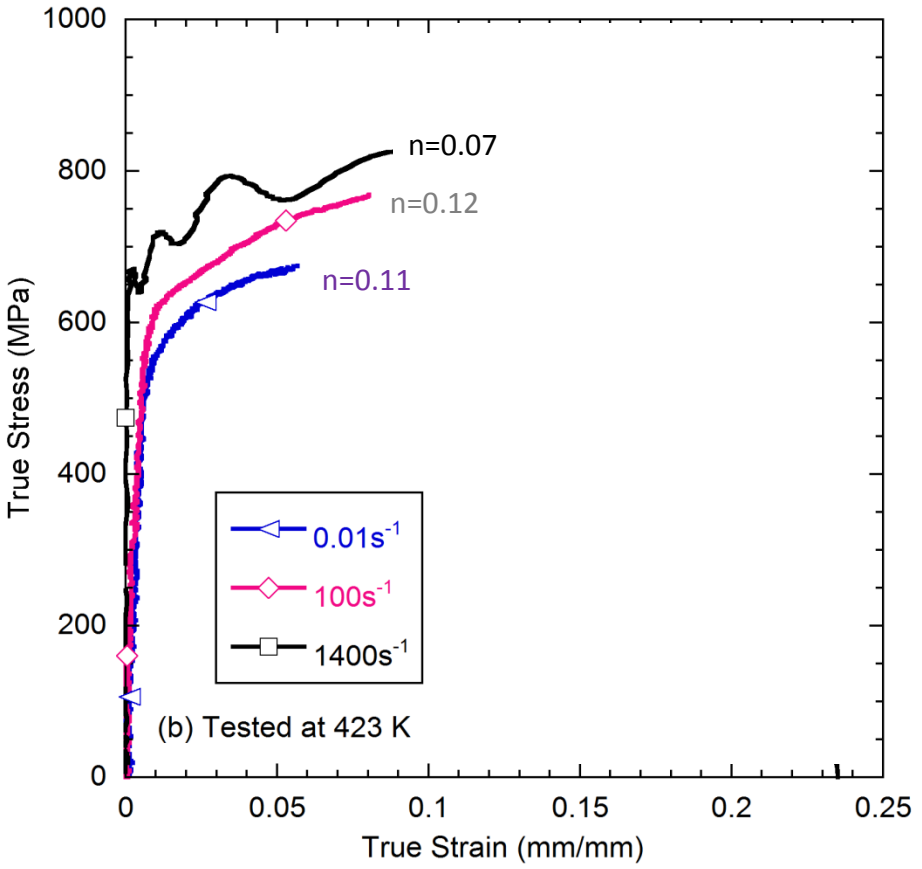

Fig. 6

(a) 296K

0.01/s 1/s 10/s 100/s 1400/s

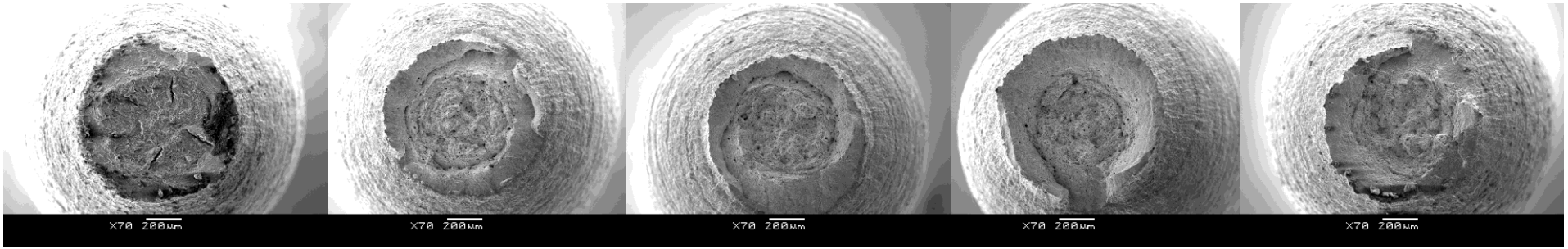

(b) 423K

0.01/s 100/s 1400/s

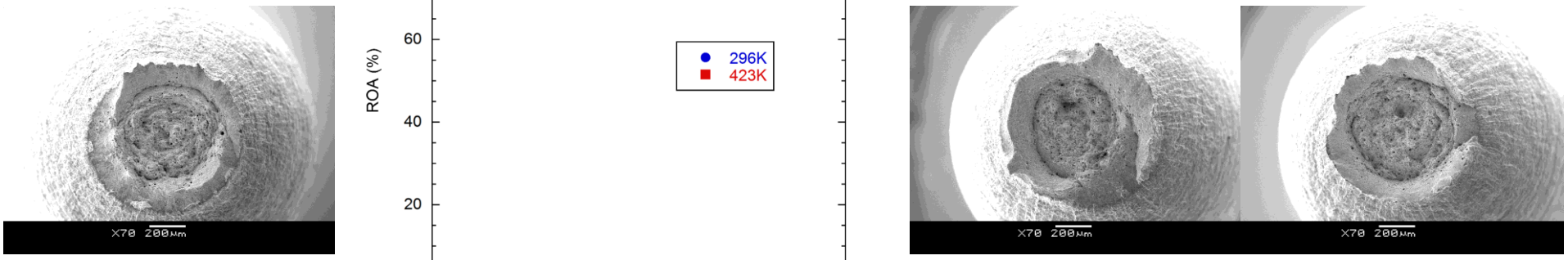

c) Reduction of area (ROA)

Fig. 7

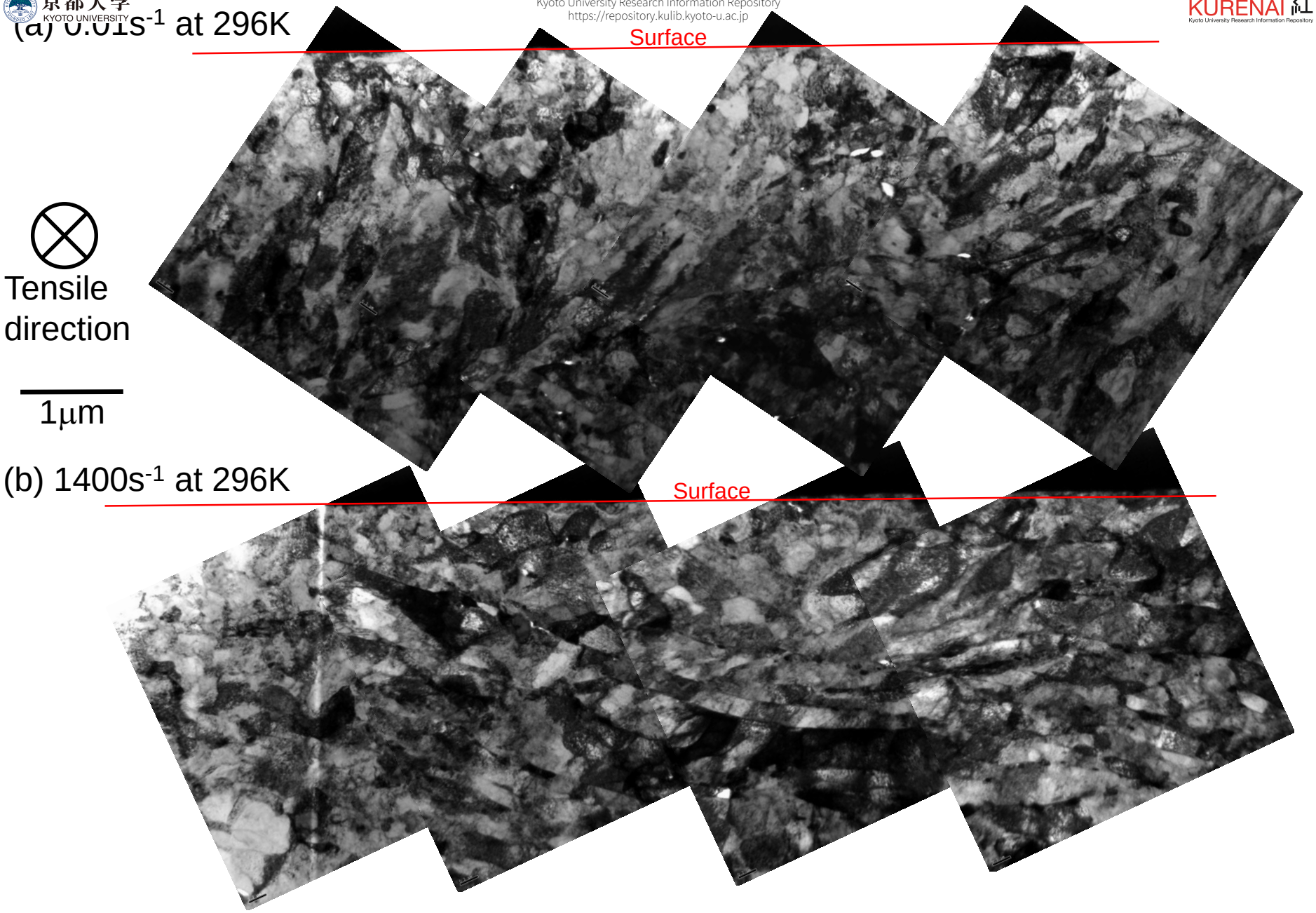

Fig. 8

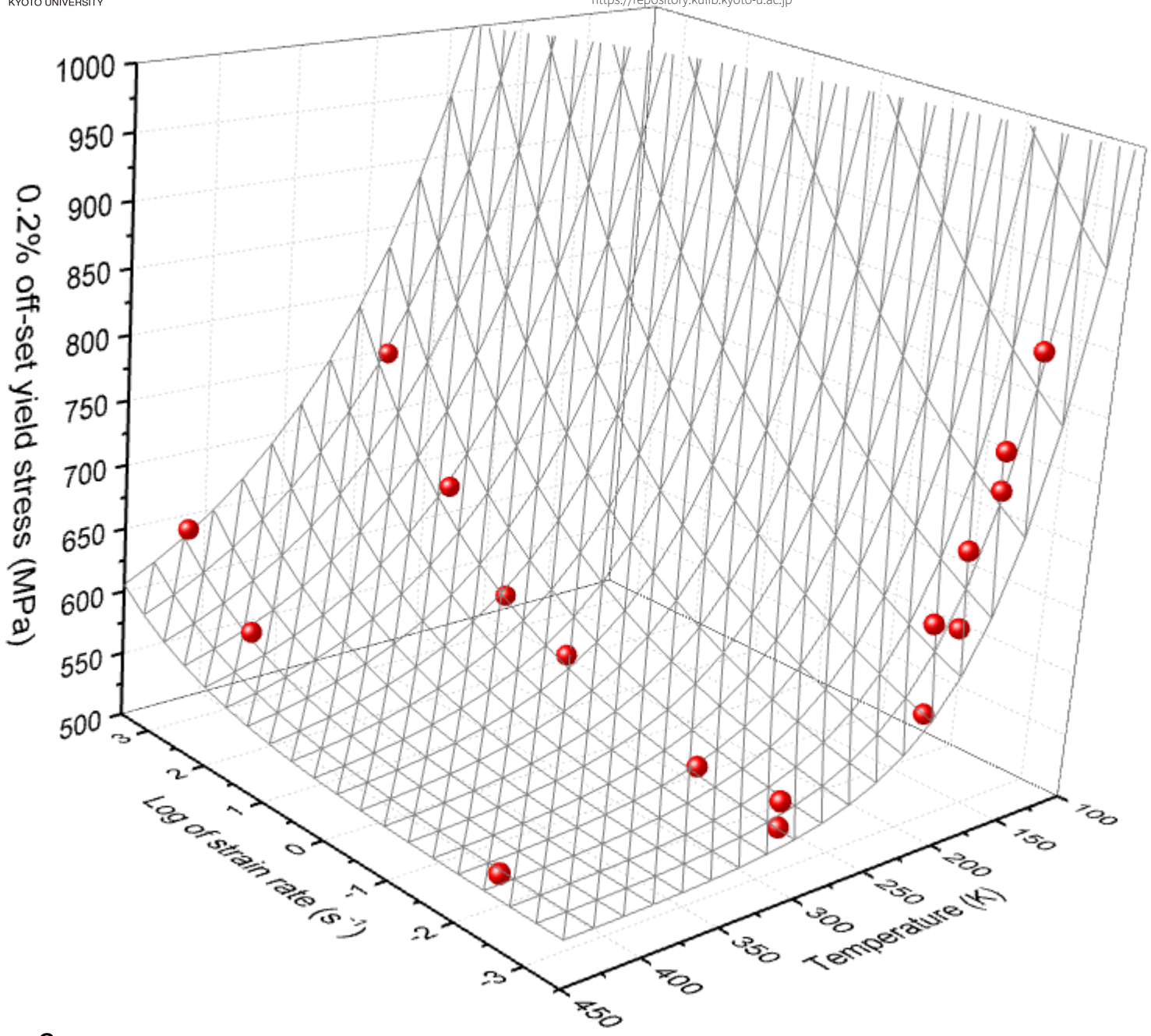

Fig. 9